Detecting Steel Cord Discontinuities in Tire Tread X-Ray Images: A Preliminary Study

Gábor Lékó and Péter Balázs
Department of Image Processing and Computer Graphics
University of Szeged
Árpád tér 2, H-6720, Szeged, Hungary
{leko,pbalazs}@inf.u-szeged.hu

***Abstract*—During the manufacturing of tires or due to excessive use, steel-cord belt plies may get damaged, single wires or even entire cords may break. Steel cord discontinuities do not always cause visibly detectable degeneration on the surface of the tire, nevertheless, in these cases non-destructive testing methods can still reveal defects inside the tire. In this paper we propose a simple yet efficient method to detect discontinuities of steel-cord belt plies in the tread area of tires, using automatic analysis of X-ray images.**

***Index Terms*—automatic tire inspection, steel cord discontinuity, x-ray**

I. Introduction

Tire manufacturing is a complicated process where many components are used to build the different parts. In this study, the important parts are the *Tire tread* which is the portion of the tire that comes in contact with the road, the *Tire belts* which are rubber-coated layers of steel, fiberglass, rayon, and other materials located between the tread and plies, and the *Tire bead* which are rubber-coated loops of high-strength steel cable (see also Fig. 1).

Quality control is an essential part of the tire manufacture. It can consist of visual inspection, check for imbalance, force variation control, and X-ray control. The latter one is suitable to detect impurities, air bubbles or discontinuities in the interior of the tire. X-ray images are often analysed by human observers which may result in misjudgement of the tire. To improve the speed and efficiency, automatic detection methods, using image processing and artificial intelligence shall be developed. Defects in the sidewall can be detected by many different approaches (see, e.g., [1]–[5]). However, there are just few references discussing the detection of defects in tread area. In [6], the authors proposed a detection method based on the feature dissimilarity analysis, which can locate the defects (such as impurity, bubble, and overlap) of tire images and outperforms the traditional defect detection algorithms in terms of various quantitative metrics. In [7], the authors describe a detection method which also can be applied in the tread area, but it is limited to crack detection.

In this paper we focus on detecting broken or missing wires in the tread region, by an automatic radiographic analysis. To our knowledge this type of failure has not been investigated yet, even in [7] only failures caused by impurities and overlaps were studied. Here, as a preliminary study, we provide a simple yet efficient method to solve the problem. The structure of the paper is the following. In Section II, we describe how the tire X-ray images are produced. In Section III, we give a detailed description of the proposed method and its implementation. Then, in Section IV, we present our experimental results. Finally, Section V is for the conclusion.

II. The Imaging Process

We use the prototype X-ray scanner presented in [8] and produce X-ray images from two different angles (70°and 110°), while the tire is fully rotated. Thus, we obtain two outstretched 2D images of the examined object. The chosen angles guarantee that the whole tread (the part of the tire where the steel cords are present) is covered. The 70cm wide line-detector contains 5566 pixels with 12 bit quantization ensuring a submillimeter spatial resolution. The width of a raw X-ray image is always 5566 pixels, while the height depends on the diameter of the tire. Fig. 1 shows an example pair of raw X-ray images, while Fig. 2 presents 3 samples taken from these images, to explain the process in detail, in the followings. (For further analysis, the images in Fig. 1(a-b) and Fig. 2 are available on the following website: http://www.inf.u-szeged.hu/~leko/pub/TireXRay/PreliminaryStudy/. The results for Fig. 1 can be seen in the first row of Table I, as Tire1.)

III. Proposed Method

The detection and analysis process starts with a preprocessing step where the region of interest is identified. Then we segment the steel strands and perform a morphological thinning on the binarized image. We developed two different techniques for tear detection (Primary and Secondary) complementing each other.

A. Preprocessing

To reduce the size of the images to be analyzed we need a preprocessing phase to determine the region of interest which is the part between the two bead cores. The bead core is made of steel having a large linear attenuation coefficient, thus is observable as dark vertical strips in the image. It can be extracted using a global segmentation, since intensities in this part are close to the minimum. After finding the two biggest

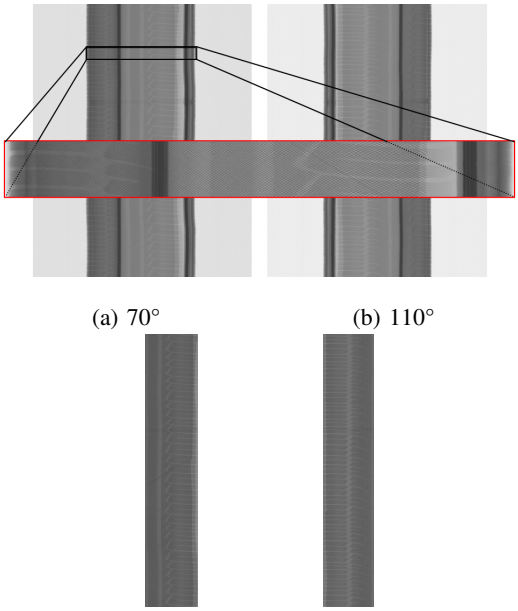

(a) 70° (b) 110°

(c) 70°- cropped (d) 110°- cropped

Fig. 1. (a-b) Raw X-ray images with a magnified part in the red rectangle. (c-d) The same images after cropping the region of interest

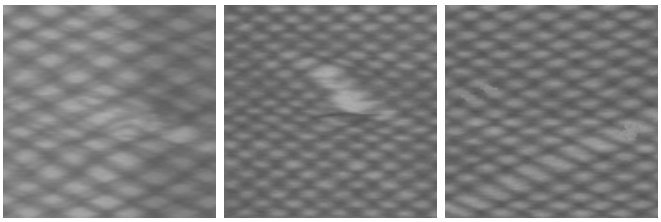

(a) Sample no. 1 (b) Sample no. 2 (c) Sample no. 3

Fig. 2. Sample images

connected components corresponding to the bead core on the left and on the right, we crop the intermediate area (see Fig. 1c-d).

B. Segmentation of the steel cord strands

To segment steel cord strands we designed a special convolution mask, based on the idea that in different tires the strands are embedded in similar orientations. By conducting numerous experiments, we succeeded to design a general convolution mask which worked properly on each test data investigated, and proved to be generally appropriate for our purposes. The mask has a rectangular shape and its size is 14×27 pixels. It distinguishes two different regions: diagonal and background points (Fig. 3). The width of the diagonal is 4 pixels. Formally, the mask $M_{14\times 27}$ is defined as follows. For an arbitrary point (i, j) of the mask

$$M(i,j) = \begin{cases} \text{-1, if } (i,j) \text{ is a background pixel} \\ \#bg/\#d \ , \ \text{otherwise,} \end{cases} \quad (1)$$

where $\#bg$ ($\#d$) denotes the number of background (diagonal) points respectively. In our case $\#bg = 283$ and $\#d = 95$.

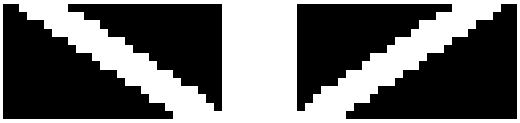

Fig. 3. Convolution masks (enlarged)

Therefore, the value of the fraction in (1) is 283/95 = 2.9789. The sum of the mask point values equals zero.

Of course, the resulting mask will highlight the lines only in one direction. We can enhance the lines in the other direction with the vertical flip of M, using the same method. Thus, in the end, the lines with the direction of the two diagonals will be highlighted (see first column of Fig. 5).

After the convolution, the intensities of the metal threads will be sufficiently different from the background intensities. Now, we perform an adaptive segmentation on the convolved images to binarize them. In the X-ray images there can be regions without metal strands. They remain homogeneous even after the convolution. The standard deviation of the pixel values in a predefined window (in our case, of size 50×50) centered at the pixel of a homogeneous region is low. Therefore, if we treat the points with low standard deviation as background points and keep only points of the image with high standard deviation, we can maintain the steel strand lines and delete the rest of the image (see second column of Fig. 5).

C. Thinning and extraction of the steel strands profile

The segmentation of the convolved images results in binary images which indicate the steel strands with white pixels. However, not every white pixel corresponds to a steel strand point. In this form, the phenomenon of the tear cannot be precisely identified yet. We could easily classify some white pixels wrongly as strand points which, in fact, belong to discontinuities. Thus, we have to examine the steel strands as one-point thick lines. For this, we perform a midline thinning on the binary images followed by a morphological pruning to remove short branches [9]. As a result, metal strands become one-point thick lines (see third column of Fig. 5).

Due to the fact that the tires often contain more than just two steel cord belt plies, it may happen that the plies are overlapped, or the metal strands appear side by side along the tire in the same direction, or even the twisted metal strands may slip apart (Fig. 4). In this case, the midline thinning is likely not to give a satisfying result, namely, the one-point thick lines do not exclusively consist of steel strand points. Thus, an additional method is necessary.

For all the points along the extracted midlines, we identify the perpendicular neighbor points. When at least one neighbor pixel has a lower intensity than the actual midline point has, we replace the midline point with the pixel having the lowest intensity, among the investigated neighbors. As a result, we get non-connected but consecutive point sequences, which contain all the points with the lowest intensities, running across the metal strands. We call this process as extended thinning (see fourth column of Fig. 5).

Fig. 4. Doubled metal threads

D. Primary tear detection

After the midline thinning, we can reveal tears which are relatively long, or even shorter ones provided the steel strand is bent. Indeed, in these cases, broken strands can be detected as disconnected lines. It is easy to find the endpoints and the branch points of a one-pixel wide line. A point will be an endpoint if it has only one foreground neighbor and will be a branch point if it has at least three foreground neighbors. If endpoints or branch points are located not close to the borders of the image, they indicate tears in the metal strands.

E. Secondary tear detection

In order to find shorter tears, we first have to determine which points belong to the background and which to the foreground. Due to the pattern of the tires we have to treat each image point differently. Moreover, the images are often noisy and cannot be enhanced using general filtering methods, namely, the tears could be easily blurred which could complicate their detection.

We propose the following algorithm for extracting the background and foreground images. We first perform a basic segmentation on the raw X-ray images. The resulted binary image is considered to define the initial sets of the foreground (object) and background pixels. After a dilation on the foreground pixels, we calculate new intensity values for all the foreground positions in the original grayscale image. For this we use linear interpolation, based on the contour points of the foreground regions. The same procedure is performed on the background points. After an average filtering we get two smooth images. The first one contains the background intensities, which varies by region, based on the source X-ray image, and the second one contains the same information about the foreground intensities (Fig. 6).

Using the background and foreground images we can analyze each point resulted in the extended thinning step, and classify them by investigating whether their intensity is closer to the background or to the foreground intensity, i.e.,

$$distOrigFg(i,j) = abs(orig_{int(i,j)} - fg_{int(i,j)}) \ , \qquad (2)$$

$$distOrigBg(i,j) = abs(orig_{int(i,j)} - bg_{int(i,j)}) \ , \qquad (3)$$

$$classify(i,j) = \begin{cases} \text{tear, if } distOrigFg(i,j) > distOrigBg(i,j) \\ \text{metal thread, otherwise,} \end{cases} \qquad (4)$$

where $orig_{int(i,j)}$ denotes the original intensity, $fg_{int(i,j)}$ and $bg_{int(i,j)}$ is foreground and background intensity in the (i,j) position, respectively. As a final step all the points classified as tear points and having no tear point neighbors are considered as noise and eliminated from the tear points.

IV. Results

The output of the process is an image marked by colored circles at the possible position of the tears (see Fig. 7). Analysing this, an expert can decide whether these are real tears or not.

To evaluate the methods we calculated the precision and recall measures [10], [11]. Denoting the number of True positive, False positive, True negative, and False negative examples by TP, FP, TN, and FN, respectively, they are given by

$$Recall = \frac{TP}{TP+FN} \quad \text{and} \quad Precision = \frac{TP}{TP+FP} \ . \qquad (5)$$

Our aim was to maximize Recall, because it is not acceptable to classify a tire as perfect if it contains tears. Precision is of less importance in our case, because - as we mentioned - after our designation a specialist will decide whether there is a real tear or not. Table I presents the calculated values together with the running time of the analysis, using X-ray images of five tires. The number of broken strands is given in the second column. The X-ray images of Tire 1-4 were manipulated by creating 16-16 artificial defects using an image processing software. Tire 5 contained 16 artificial and 12 real broken strands. Recall is 1.0 in each case which shows that no real tear is lost. High Precision values also show that the majority of the indicated discontinuities are indeed real tears. Thus, in summary, the developed automatic method can greatly help the experts in detecting the steel cord tears. From a practical point of view, the running time seems to be acceptable, too. Nevertheless, it could be further sped up with code optimization or parallel processing techniques, for example.

TABLE I
Results

	Tears[nr]	Recall [%]	Precision [%]	Runtime [sec]
Tire1	16	1.000	0.941	326
Tire2	16	1.000	1.000	233
Tire3	16	1.000	0.889	351
Tire4	16	1.000	1.000	267
Tire5	28	1.000	0.966	278
Average		1.000	0.959	291

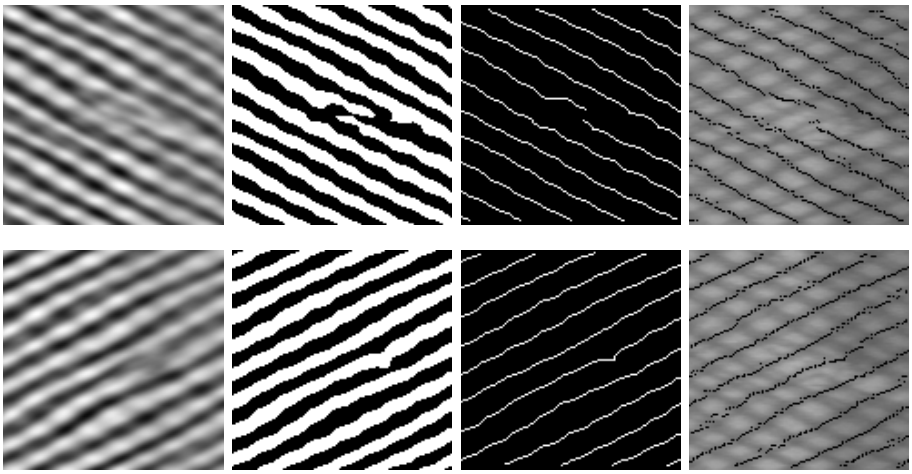

(a) Sample image no. 1

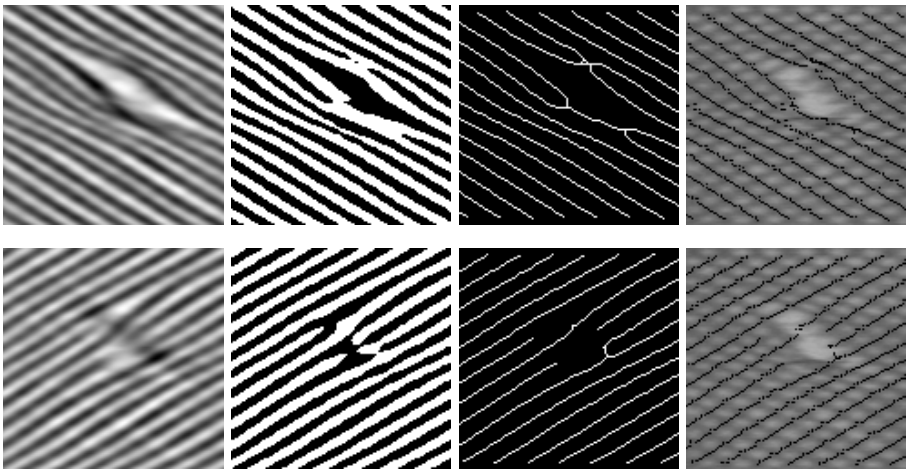

(b) Sample image no. 2

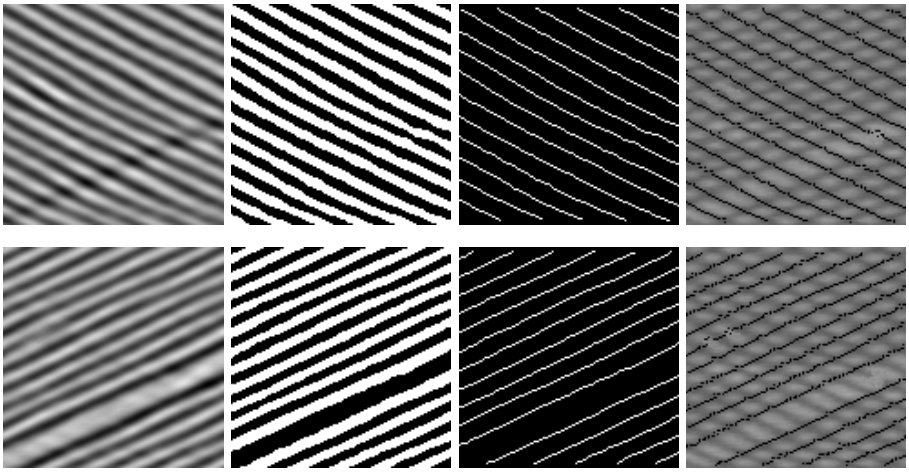

(c) Sample image no. 3

Fig. 5. The steps of the detection process on the sample images of Fig. 2. From left to right: convolution, segmentation, thinning, extended thinning

Fig. 6. Background and foreground images extracted from Sample image no. 1

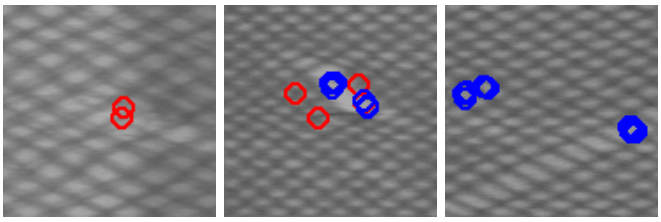

(a) Sample no. 1 (b) Sample no. 2 (c) Sample no. 3

Fig. 7. Results - Red: primary tear detection, Blue: secondary tear detection

V. Conclusion

In this paper we described an automatic method to localize tears in steel cords of tires of the tread region, using X-ray images. The method uses image processing techniques to find the defects. For the evaluation of the proposed solution, we conducted experiments on X-ray images of different tires. We found that the method can find the tears in all the cases, and just rarely results in false positive evaluations, which can be easily selected out by an expert. Thus, a promising and efficient tool is developed to help quality control in tire manufacturing.

The paper presents a preliminary study. In our future work we plan to conduct a thorough experiment using also other measures to evaluate our results. We intend to increase the value of precision, incorporating further knowledge about the metal strands and their possible tears. A fast implementation is also among our future plans. We noticed that the running time is mostly affected by processing the foreground and background images, due to the linear interpolation. Thus, as a first step, this part of the algorithm should be revisited.

Acknowledgments

The authors thank the GriffSotf ZRT company for providing access to their 3D Tire Scanner and Gábor Petrovszki for his generous help in the scanning process. The research was supported by the NKFIH OTKA [grant number K112998].

References

[1] Y. Zhang, D. Lefebvre, Q. Li: Automatic detection of defects in tire radiographic images, IEEE Transactions on Automaton Science and Engineering, Vol.: PP, Issue: 99, pp. 1–9, DOI: 10.1109/TASE.2015.2469594 (2015).

[2] Q. Guo, Z. Wei: Tire defect detection using image component decomposition. Research Journal of Applied Sciences, Engineering and Technology 4(1) 41–44 (2012).

[3] Y. Zhang, T. Li, Q.L. Li: Defect detection for tire laser shearography image using curvelet transform based edge detector. Optics and Laser Technology 47 64–71 (2013).

[4] Y. Zhang, T. Li, Q.L. Li: Detection of foreign bodies and bubble defects in tire radiography images based on total variation and edge detection. Chinese Physics Letters 30(8), Article ID 084205 (2013).

[5] Y. Xiang, C. Zhang, Q. Guo: A dictionary-based method for tire defect detection. Proceedings of the IEEE International Conference on Information and Automation (ICIA '14), pp. 519–523, Hailar, China, July 2014.

[6] Q. Guo, C. Zhang, H. Liu, X. Zhang: Defect detection in tire x-ray images using weighted texture dissimilarity. Journal of Sensors, Article ID 4140175 (2016).

[7] L. Jinping, H. Wendi, H. Yanbin, Y. Jianqin: Crack detection in tread area based on analysis of multi-scale singular area. Communications in Computer and Information Science 547 201–218 (2015).

[8] P. Balázs, G. Lékó, Z. Ozsvár, G. Petrovszki, J. Szűcs, L. Varga: Design and implementation of the informatical system of a 3D industrial CT scanner. Abstracts of the 11th Conference of the Hungarian Association of Image Processing and Pattern Recognition, Sovata, Romania, 24-27 January, pp. 1–10 (2017) (in Hungarian).

[9] T.Y. Kong, A. Rosenfeld: Topological Algorithms for Digital Image Processing. Elsevier Science, Inc., 1996.

[10] J. Davis, M. Goadrich: The relationship between precision-recall and ROC curves. Proceedings of the 23rd International Conference on Machine Learning, Pittsburgh, PA, pp. 233–240 (2006).

[11] D.M.W. Powers: Evaluation: from precision, recall and F-factor to ROC, informedness, markedness and correlation. International Journal of Machine Learning Technology 2 (1), 37–63 (2011).